1-1-2020

Seismic performance of concrete-filled SHS column-to-beam connections with slip-critical blind bolts

Weifeng Jiao

Wei Wang

Yiyi Chen

Lip H. Teh
University of Wollongong, lteh@uow.edu.au

Seismic performance of concrete-filled SHS column-to-beam connections with slip-critical blind bolts

Abstract

© 2020 Elsevier Ltd This paper investigates the use of slip-critical blind bolts to connect I-beams to concrete-filled steel square hollow section (SHS) columns. The strength and stiffness of the resulting joints are determined experimentally for the purpose of classifying them according to the Eurocode. Their suitability for use in special moment frames is also assessed through cyclic bending tests. Three types of beam sections are tested, being a compact welded section, a reduced beam (flange) section, and a reduced beam section with concrete slab at the top. All tested joints are full strength according to the Eurocode, allowing the connected beams to reach their respective plastic moment capacities. In addition, they are rigid for braced and unbraced frames, except for the reduced beam section specimen, which are semi-rigid only for unbraced frames according to the Eurocode. However, all specimens have sufficient ductility to be used in special moment frames, with no pinching effect in their hysteretic moment-rotation curves. Their initial rotational stiffness is dominated by the stiffness of the column flange in bending, which can be conservatively estimated using the formulation presented in this paper.

Disciplines

Engineering | Science and Technology Studies

Publication Details

Jiao, W., Wang, W., Chen, Y. & Teh, L. (2020). Seismic performance of concrete-filled SHS column-to-beam connections with slip-critical blind bolts. Journal of Constructional Steel Research, 170

Seismic performance of concrete-filled SHS column-to-beam connections with slip-critical blind bolts

Weifeng Jiao [a,b], Wei Wang [a, b, *], Yiyi Chen [a, b], Lip H. Teh [c]

[a] *State Key Laboratory of Disaster Reduction in Civil Engineering, Tongji University, Shanghai 200092, China*
[b] *Department of Structural Engineering, Tongji University, Shanghai 200092, China*
[c] *School of Civil, Mining & Environmental Engineering, ARC Research Hub for Australian Steel Manufacturing, University of Wollongong, Wollongong, NSW 2522, Australia*
** Corresponding author: email: weiwang@tongji.edu.cn, Tel: +86 (0)21-65982926*

Abstract: This paper investigates the use of slip-critical blind bolts to connect I-beams to concrete-filled steel square hollow section (SHS) columns. The strength and stiffness of the resulting joints are determined experimentally for the purpose of classifying them according to the Eurocode. Their suitability for use in special moment frames is also assessed through cyclic bending tests. Three types of beam sections are tested, being a compact welded section, a reduced beam (flange) section, and a reduced beam section with concrete slab at the top. All tested joints are full strength according to the Eurocode, allowing the connected beams to reach their respective plastic moment capacities. In addition, they are rigid for braced and unbraced frames, except for the reduced beam section specimen, which are semi-rigid only for unbraced frames according to the Eurocode. However, all specimens have sufficient ductility to be used in special moment frames, with no pinching effect in their hysteretic moment-rotation curves. Their initial rotational stiffness is dominated by the stiffness of the column flange in bending, which can be conservatively estimated using the formulation presented in this paper.

Keywords: beam-to-column connection; blind bolt; concrete-filled steel tube; cyclic behavior; initial rotational stiffness.

1. Introduction

Welded connections are often used for steel tubular members as the shape does not render itself suitable for conventional bolted connections, which are commonly used for open sections such as channel or I-sections. However, welded frame moment connections have been found to be vulnerable to premature fractures during earthquake including fractures in the beam and column sections

[1]. Flowdrill connectors [2-4] and blind bolting [5-7] have therefore been developed to avoid welding of beam-to-tubular column connections.

The flowdrill system appeared early, using high strength steel bolts with full threads. France et.al [2-4] conducted laboratory tests on rectangular hollow section (RHS) column to I-beam joints using flowdrill connectors. The effects of joint types, concrete infill in the tube and end-plate types were investigated. The results indicated the feasibility of using bolted connections for RHS columns with the flowdrill system. However, this technique was only suitable for RHS tubes with wall thickness ranging from 5 mm to 12.5 mm [8], restricting the application to low-rise steel frame structures [9].

Other types of blind bolts have also been developed, such as high-strength blind bolt (HSBB), Ultra-Twist bolt and extended hollo-bolt (EHB) [5-7]. Korol et al. [5] proposed a bolted end-plate connection between wide-flange I-beam and RHS column by using HSBBs. The experimental results indicated that the behavior of connections with HSBBs was similar to that with A325 bolts. Tabsh and Mourad [6] discussed the effects of different load combinations on the ultimate tension load of an Ultra-Twist bolt. The tensile behaviour of EHB was studied by Pitrakkos and Tizani [7].

A more recent development involves the use of “hollo-bolt” [10-19]. Mesquita et al. [15] found that the failure of hollo-bolt legs in an I-beam-to-SHS column connection caused by the bending moment adversely affected the joint stiffness. However, Wang et al. [12, 13] found that the hollo-bolt leg failure could be avoided if the tubular column was concrete filled. In addition, the behavior of blind bolted concrete-filled RHS column splice joints subjected to eccentric tension [18] and eccentric compression [19] have also been investigated, and hollo-bolt leg failures were not observed either.

Although various types of blind bolting have been developed, Wang et al. [20] have found that none of them is able to achieve slip-critical (friction-type) bolted connections except for the Ajax ONESIDE system. A novel slip-critical blind bolt (SCBB) system has therefore been developed at

Tongji University [20-21]. However, no experimental test was conducted to verify the system's performance in sustaining the full plastic moment of the beam.

In this paper, three types of beams are investigated for their performance (and the joint's) under reverse cyclic loading, which can be expected during severe earthquake. The first beam is a welded section of Class 1 cross-section classification according to EN 1993-1-1 [22]. The second beam is a reduced beam section in the shape of dog bone. The third beam is also a reduced beam section, but with a restraint from the reinforced concrete slab at the top flange. The initial stiffness, hysteretic behavior, failure mode and capacity of each beam-to-column connection are presented and discussed.

2. Specimen configurations, test set-up and loading protocol

The slip-critical blind bolt (SCBB) system comprises five parts as shown in Fig. 1: a tor-shear bolt shank [23], a split-type spacer, a shear sleeve, a normal (solid) washer and a nut. The installation procedure has been described by Wang et al. [20], as illustrated in Fig. 2. In the present experimental program, four pairs of M24 SCBBs were used to connect an I-beam to a concrete-filled SHS column via an extended end-plate that was reinforced with stiffeners, as depicted in Fig. 3.

The configuration details of the three test specimens are summarised in Table 1. The variables b_c, t_c and L_c are the width, wall thickness and length of the square column, respectively. The variables h_b and b_b are the depth and width of the beam, respectively, while t_{wb} and t_{fb} are the thicknesses of the web and flange, respectively. Specimen CB1 was compact, intended to develop the full plastic moment capacity of the beam without local buckling. Specimen CB2 used a dog-bone beam section as depicted in Fig. 4, intended to develop a plastic hinge away from the joint. Specimen CB3 benefitted from the lateral restraint provided by the reinforced concrete (RC) slab to the dog-bone beam section.

The effective width and thickness of the RC slab are 1640 mm and 120 mm, respectively. The diameter of steel bar is 8 mm, and its arrangement is shown in Fig. 5 with the same spacing for the top and bottom of the slab. In order to meet the full shear connection criteria recommended in GB

50010-2010 [24], steel shear studs with a diameter of 16 mm and a height of 88 mm were used. Two lines of steel shear studs were welded to the top flange of steel beam.

The beams, columns and connection plates were made of Q345 steel with a nominal yield stress of 345 MPa. The measured yield stress F_y and tensile strength F_u of each component are given in Table 2. The average compressive strength f_c of the concrete slab and concrete infill was 28.4 MPa as found from the compression tests of three 150-mm concrete cubes after 28 days of curing. Given the dimensions and material properties, all three specimens should satisfy the requirements for strong column-weak beam design in accordance with GB 50011-2010 [25]. Each specimen was therefore expected to fail in the beam and not the column.

The three specimens have similar test set-ups, as shown schematically in Fig. 6(a) for Specimens CB1 and CB2. For Specimen CB3, the external lateral restraints were removed. A photograph of Specimen CB3 under testing is shown in Fig. 6(b). It can be seen that two beams were connected to the concrete-filled SHS column for each specimen, which were symmetrical about the column but were loaded anti-symmetrically (see Fig. 9a). The beams were located at 1675 mm from the column base.

In order to achieve pinned connections at both ends of the column, spherical hinges were used at the top and the bottom of each column. The column top was loaded with a hydraulic jack for axial compression. As indicated in Fig. 6, two hydraulic actuators were used to apply cyclic loads at the ends of the beams. The distance from each beam end to the centre of the column is 1800 mm.

In each test, the axial compression of the column was applied first and kept constant throughout the cyclic loading of the specimen (beams). The cyclic loading was conducted in accordance with Section K2.4b of AISC 341-16 [26], as defined in Fig. 7 for the present specimens.

The locations of the linear variable displacement transducers (LVDT) and strain gauges are shown in Fig. 8. The transducers not only measured translations, but also enabled the calculation of rotations as needed. The shear deformation of the panel zone was measured by the diagonal transducers inside the zone.

Although a horizontal brace was provided to restrain the spherical hinge at the top of the column as shown in Fig. 6, the top (and bottom) of the column was not completely restrained from moving horizontally. The column was therefore subject to (in-plane) rigid body rotation, which necessitated the placement of transducers at the top and bottom of the column, as indicated in Fig. 8.

Fig. 9 defines the inter-storey drift θ for the two extreme scenarios: (a) no rigid body rotation of the column, and (b) no rigid body rotation of the pair of beams. In the presence of both rigid body rotations, the inter-storey drift can be determined by superposition. Note that the chords of the beams and columns are not shown in Fig. 9 for legibility.

3. Experimental results

All the strong column-weak beam specimens failed by fracture of the beam flange. However, the exact structural responses were different among them as described in the following.

It was found from the strain gauge readings of Specimen CB1 that the connected end of the beam started to develop plasticity when the inter-storey drift θ approached 0.015 rad, which spread to the whole depth of the web at 0.03 rad to form a plastic hinge. The flanges buckled in the first cycle at 0.05 rad followed by the web in the second cycle, as shown in Fig. 10(a). Fracture of the flange took place in the next cycle at 0.06 rad, as shown in Fig. 10(b).

The reduced beam section of Specimen CB2 also became fully plastic at 0.03 rad, but one of the beam buckled torsionally at 0.04 rad as indicated in Fig. 11(a). The torsional buckling led to an earlier fracture compared to Specimen CB1, at about 0.05 rad. The complete fracture of the top flange of the reduced section is shown in Fig. 11(b).

As the neutral axis of Specimen CB3 was located further from the bottom flange due to the presence of the concrete slab connected to the top flange by shear studs, yielding started in the bottom flange at about 0.01 rad, earlier than the other two specimens. Significant local buckling deformations of the bottom flange and web could be seen when 0.05 rad was being approached, as shown in Fig. 12(a). Cracking of the bottom flange was observed at 0.06 rad, accompanied by concrete crushing around the column as shown in Fig. 12(b). Fracture of the bottom flange was complete by 0.07 rad as shown in Fig. 12(c).

In all the three tests, the SCBB connections remained tightened throughout without visible relaxation, as evident from Figs. 13 and 14. It was therefore concluded that the SCBB connections met the requirements for being slip-critical.

Fig. 14 shows the hysteretic moment-rotation curves of the three beam-to-column joints. The robustness of the SCBB connection is apparent from the absence of pinching in all three curves. Figs. 14(a) and 14(b) exhibit the "well-behaved" hysteretic responses of Specimens CB1 and CB2, where energy was evenly absorbed through inelastic deformations in both directions of bending. However, due to the presence of the concrete slab at the top flange of Specimen CB3, the energy was absorbed differently between positive and negative bending.

The hysteretic moment-rotation curves of Specimens CB1 and CB2 in Fig. 14 were plotted for the respective beams that fractured. The positive moment is defined to be the sagging moment, as the hogging moment is negative. For Specimen CB3, the concrete slab was in compression under the positive moment. Only the response of the right beam of Specimen CB3 was used in Fig. 14 as the concrete did not crush in the same number of cycles.

4. Analysis of experimental responses

4.1 Initial stiffness and classification of joints

According to EN 1993-1-8 [27], a joint is classified by stiffness and by strength. With respect to strength, it has been demonstrated through the experimental tests described in the preceding section that the SCBB connections were able to sustain the plastic moment of the connected beams, and the tested joints were therefore full-strength joints.

The initial rotation θ_j of the SCBB connection, i.e. the initial change in the angle between the beam and the column, can be computed by subtracting the elastic rotations θ_b of the beam and θ_c of the column from the inter-storey drift θ obtained from the transducers. The elastic rotation θ_b of the beam is determined using classical structural mechanics:

$$\theta_b = \frac{PL^2}{12EI_b} \tag{1}$$

in which E is the elastic modulus, I_b is the second moment of area of the beam, P and L are defined in Fig. 9. Likewise, the elastic rotation θ_c of the column is

$$\theta_c = \frac{P(H_1^3 + H_2^3)}{3EI_c} \cdot \frac{L}{H^2} \tag{2}$$

in which I_c is the second moment of area of the column, while H, H_1 and H_2 are defined in Fig. 9.

The classification of a joint into a rigid one or otherwise is not only a function of the connection stiffness, but is also dependent on the frame's type (unbraced or braced) and topology. In the present work, the ratio of the beam span L_b to its depth is assumed to be 20, which is representative of a light weight steel structure. Table 3 compares the measured initial rotational stiffness $S_{j,ini}$ of the present specimens against the rigid joint thresholds set in Section 5.2.2.5 of EN 1993-1-8 [27] for unbraced and braced frames. It is seen that all three SCBB connected joints were rigid for braced frames, and CB1 and CB3 were also rigid for unbraced frames.

4.2 Ductility assessment

According to Section E3 of AISC 341-16 [26], the inter-storey drift $\theta_{0.8}$ of a beam-to-column joint used in a special moment frame (SMF) should not be less than 0.04 rad when the flexural resistance of the joint equals 80% of the beam's plastic moment capacity. The inter-storey drift $\theta_{0.8}$ of the present specimens are determined from their backbone curves plotted in Fig. 15. Table 4 shows that all three SCBB specimens satisfy the ductility requirement for a special moment frame.

4.3 Stiffness degradation

During cyclic loading, the stiffness of each specimen decreased progressively because of the accumulation of inelastic deformation. The stiffness degradation is characterised by the factor λ_i, which is the ratio K_i/K_1, where K_i is the secant stiffness of the first complete cycle at the i^{th} load step with the same drift θ [28]:

$$K_i = \frac{|+F_i| + |-F_i|}{|+X_i| + |-X_i|} \tag{3}$$

in which the variable F_i is the peak load in a particular direction, and X_i is the corresponding displacement.

Fig. 16 shows that there were no significant differences in stiffness degradation between Specimens CB1 and CB2, the latter having a reduced beam section. For Specimen CB3, two separate plots were used for positive bending and negative bending due to asymmetry about the neutral axis. The two plots were quite different from each other, and from those of the other two specimens. It is interesting to note that up to 3.5% drift (0.035 rad), the stiffness degradation of Specimen CB3 under negative bending was less severe than all others.

4.4 Energy dissipation

The ability of a structural component to dissipate energy can be represented by the equivalent viscous damping ratio ζ_{eq}, computed from

$$\zeta_{eq} = \frac{1}{2\pi} \cdot \frac{S_{(ABC+CDA)}}{S_{(OBE+ODF)}} \tag{4}$$

in which $S_{(ABC+CDA)}$ is the area enclosed by the hysteresis curve in Fig. 17, and $S_{(OBE+ODF)}$ is the sum of areas of triangle OBE and triangle ODF in the figure.

In the present work, the largest hysteresis loop of each specimen was used to determine its equivalent viscous damping ratio ζ_{eq}, given in Table 5. It was found that the plastic energy dissipation capacities of the steel beam Specimens CB1 and CB2 were greater than that of the composite beam Specimen CB3. The equivalent viscous damping ratios ζ_{eq} of Specimens CB1 and CB2 are 20.6% and 22.4% higher than that of Specimen CB3, respectively.

5. Analytical determination of initial rotational stiffness

The initial rotational stiffness of the studied joints can be determined by the component method specified in Section 6.3.3 of EN 1993-1-8 [27]. According to the code, for end-plate joints with two or more bolt-rows in tension, a single equivalent stiffness coefficient k_{eq} can be used to represent the components related to the bolt-rows:

$$k_{eq} = \frac{\sum_r k_{eff,r} h_r}{z_{eq}} \tag{5}$$

$$k_{eff,r} = \frac{1}{\sum_{i=1}^{5} \frac{1}{k_{i,r}}} \tag{6}$$

$$z_{eq} = \frac{\sum_r k_{eff,r} h_r^2}{\sum_r k_{eff,r} h_r} \tag{7}$$

in which h_r is the distance between bolt-row r and the centre of compression; $k_{eff,r}$ is the effective stiffness coefficient for bolt-row r taking into account the stiffness coefficients for the basic components in tension or bending; z_{eq} is the equivalent lever arm.

For bolt-row r of the present specimens, the effective stiffness coefficient $k_{eff,r}$ takes into account the stiffness coefficients of five basic components:

$$k_{1,r} = k_{wc,t,r} = \frac{0.7 b_{eff,t,wc} t_{wc}}{d_c} \tag{8}$$

$$k_{2,r} = k_{ep,t,r} = \frac{0.9 l_{eff} t_p^3}{m^3} \tag{9}$$

$$k_{3,r} = k_{bolt,t,r} = 1.6 A_s / L_{bolt} \tag{10}$$

$$k_{4,r} = k_{bar,t,r} = \frac{A_{s,r}}{(h/2)} \tag{11}$$

$$k_{5,r} = k_{fc,t,r} \tag{12}$$

The first three components are given in Section 6.3.1 of EN 1993-1-8 [27] to represent the column web in tension ($k_{wc,t,r}$), the end-plate in bending ($k_{ep,t,r}$) and the bolts in tension ($k_{bolt,t,r}$). The fourth component is given in Annexure A of EN 1994-1-1 [29] to represent the longitudinal steel reinforcement in tension ($k_{bar,t,r}$).

The fifth component represents the column flange in bending ($k_{fc,t,r}$), which is not covered in EN 1993-1-8. Hence, a new mechanical model is proposed in this paper to determine the stiffness coefficient based on the theory of plates and shells by Timoshenko [30].

In accounting for the effect of the column web on the stiffness of the column flange, only the symmetric half of the SHS tube is considered as shown in Fig. 18. The area of each bolt load is assumed to be rectangular, and the corner of the tube is simplified as right-angle. The variable b denotes the length of the tubular column influenced by the bolt loads, and the spread angle of 65° (see Fig. 19b) has been determined by numerical analysis [31].

In Fig. 19, the symmetric half of the tube is divided into one simply supported rectangular plate (column flange, Fig. 19b) under two tension forces and moments distributed along two opposite edges, and two simply supported rectangular plates (column webs, Fig. 19c) under moments distributed along two opposite edges. The locations of the bolt loads are at $x_1 = \pm\xi$, and the area of each bolt load is $u\times v$. For column flange, it can be further separated into three load cases (Fig. 19d). The first case is a simply supported plate under a uniformly distributed load over the strip corresponding to the first bolt as indicated in the left end of Fig. 19d. In Equations (13) and (14), the deflection of the plate in the region $-\xi+u/2 \leq x_1 \leq a/2$ is denoted w_{1a}. The second case corresponds to the second bolt, with w_{2a} and w_{2b} denoting the deflections in the regions $\xi+u/2 \leq x_1 \leq a/2$ and $-a/2 \leq x_1 \leq \xi-u/2$, respectively. The third case is a simply supported rectangular plate under moments distributed along two opposite edges, and the deflection is denoted w_3. Because of the symmetry, the distributed moment applied to the two opposite edges of the flange can be represented by a trigonometric series, $f_1(y)$. For the column web, the distributed moments need to be represented by two trigonometric series, $f_1(y)$ and $f_2(y)$, and its deflection is denoted w_4.

It is assumed that the angle between the flange and the web stays constant, so the deformation compatibility condition gives:

$$\left(\frac{\partial w_{1a}}{\partial x_1}\right)_{x_1=a/2} + \left(\frac{\partial w_{2a}}{\partial x_1}\right)_{x_1=a/2} + \left(\frac{\partial w_3}{\partial x_1}\right)_{x_1=a/2} = \left(\frac{\partial w_4}{\partial x_2}\right)_{x_2=-c/2} \quad (13)$$

The maximum deflection of the flange is calculated by the following equation:

$$w_{\max} = \left(w_{1a} + w_{2b} + w_3\right)_{x_1 = y = 0}$$

$$= \frac{4 q_0 b^4}{\pi^5 D} \sum_{m=1,3,5\ldots} \frac{1}{m^5} \left(L_m + \frac{\beta_m \tanh \beta_m}{\cosh \beta_m} \cdot \frac{Q_m}{R_m + \dfrac{2 S_m T_m}{T_m - S_m}} \right) \sin \frac{m\pi v}{2b} \tag{14}$$

where

$$b = \left(a - 2\xi\right) \times \tan 65^{\circ} \tag{15}$$

$$a = b_c - t_c \tag{16}$$

$$L_m = \frac{1}{\cosh \beta_m} [\gamma_{m2} \sinh\left(2\gamma_{m2} - \beta_m\right) - \cosh\left(2\gamma_{m2} - \beta_m\right) - \gamma_{m1} \sinh\left(2\gamma_{m1} - \beta_m\right)$$

$$+ \cosh\left(2\gamma_{m1} - \beta_m\right)] + \frac{\beta_m}{2\cosh^2 \beta_m}\left(\sinh 2\gamma_{m1} - \sinh 2\gamma_{m2}\right) \tag{17}$$

$$Q_m = \frac{1}{2\cosh \beta_m}\left(\beta_m \tanh \beta_m + 1\right)\left(\sinh 2\gamma_{m1} - \sinh 2\gamma_{m2}\right)$$

$$+ \frac{1}{\cosh \beta_m}\left(\gamma_{m2} \cosh 2\gamma_{m2} - \gamma_{m1} \cosh 2\gamma_{m1}\right) \tag{18}$$

$$R_m = \frac{\beta_m}{\cosh^2 \beta_m} + \tanh \beta_m \tag{19}$$

$$S_m = \frac{\alpha_m}{\cosh^2 \alpha_m} + \tanh \alpha_m \tag{20}$$

$$T_m = \frac{\alpha_m}{\sinh^2 \alpha_m} - \coth \alpha_m \tag{21}$$

$$\beta_m = \frac{m\pi a}{2b} = 2\alpha_m \tag{22}$$

$$2\gamma_{m1} = \frac{m\pi}{b}\left(\xi - \frac{u}{2}\right) \tag{23}$$

$$2\gamma_{m2} = \frac{m\pi}{b}\left(\xi + \frac{u}{2}\right) \tag{24}$$

$$u = v = d_0 \tag{25}$$

The variable d_0 is the external diameter of washer.

It has been found through numerical experimentation that the deflection $w_{\max}$ can be computed accurately with m =1, 3 and 5 only. Numerical analyses have also found that the rounded corner of a cold-formed SHS increases the flange stiffness by 10% compared to a sharp right-angle corner [31]. The stiffness coefficient $k_{fc,t,r}$ of the flange of the concrete-filled SHS column with a row of two bolts is therefore

$$k_{fc,t,r} = \frac{2P}{Ew_{\max}} = \frac{2q_0uv}{Ew_{\max}} = \frac{\dfrac{1.1\pi^5 t_c^3 uv}{24b^4\left(1-v^2\right)}}{\displaystyle\sum_{m=1,3,5} \frac{1}{m^5}\left(L_m + \frac{\beta_m \tanh\beta_m}{\cosh\beta_m}\cdot\frac{Q_m}{R_m + \dfrac{2S_mT_m}{T_m - S_m}}\right)\sin\frac{m\pi v}{2b}} \tag{26}$$

in which the flexibility contributions of the column web panel in shear and the column flange region in bolt compression are ignored as their stiffness coefficients are assumed to be infinite owing to the concrete inside the tube. The effect of the concrete infill on the column flange region in bolt tension is not taken into account in the present work.

The equivalent stiffness coefficient k_{eq} defined in Equation (5) are used for determining the initial rotational stiffness of the joint:

$$S_{j,ini} = \frac{Ez^2}{\left(1/k_{eq}\right)} \tag{27}$$

in which z is the lever arm which represents the distance from the mid-thickness of the beam flange in compression to that of the beam flange in tension.

Table 6 lists the stiffness coefficients of the five components for each of the three tested specimens. It can be seen that the effective stiffness $k_{eff,r}$ is dominated by the stiffness of the column flange in bending, $k_{fc,t,r}$, which is the fifth component. The analytical stiffness coefficients of this component, computed using the formulation in this paper, lead to initial rotational stiffnesses that are less than the experimental values, as shown in Table 7. The conservatism is due to the neglect of the effect of the concrete infill on the column flange region in bolt tension, and to the fact that the lever arm z of some specimens was actually longer than the nominal value assumed in the calculation.

6. Conclusions

This paper has presented the cyclic test results of three beam-to-column joints where slip-critical blind bolts were used to connect I-beams to concrete-filled steel SHS columns through extended end-plates. All the beams were able to reach their respective plastic moment capacities, meaning that the specimens satisfied the strong column-weak beam design.

The use of slip-critical blind bolts not only rendered the three joints being full strength, but also enabled them to be classified as rigid joints in a braced frame according to the Eurocode. The specimens with full section and composite beams were also rigid for unbraced frames.

The test results demonstrated that the use of slip-critical blind bolts led to robust seismic performance of all beam-to-column joints, which exhibited sufficient ductility for use in special moment frames. There was no pinching in the hysteretic moment-rotation curves, indicating no loss in stiffness due to bolt slippage.

The analytical formulation shows that the initial rotational stiffness of all three joints were dominated by the stiffness of the column flange in bending. Accuracy in determining the latter is therefore critical to the success of estimating the former. The formulation presented in this paper can be used to estimate the stiffness coefficient conservatively, but the complete effects of the concrete infill in the tube should be studied for future refinement.

7. Acknowledgements

The financial supports from the Natural Science Foundation of China (NSFC) with Grant Nos. 51778459 and 51820105013 are gratefully acknowledged. Funding supports received from the State Key Laboratory of Disaster Reduction in Civil Engineering, Tongji University (Project No. SLDRCE19-B-05) and Sustainable Structural Engineering Research Funds from Tongji Architectural Design (Group) Co. Ltd. for the study are also gratefully acknowledged.

8. References

[1] Popov E.P., Takhirov S.W., 2002. Bolted large seismic steel beam-to-column connections Part 1: experimental study. *Engineering Structures*, 24, 1523-1534.

[2] France J.E., Davison J.B., Kirby P.A., 1999. Strength and rotational response of moment connections to tubular columns using flowdrill connectors. *Journal of Constructional Steel Research*, 50, 1-14.

[3] France J.E., Davison J.B., Kirby P.A., 1999. Strength and rotational stiffness of simple connections to tubular columns using flowdrill connectors. *Journal of Constructional Steel Research*, 50, 15-34.

[4] France J.E., Davison J.B., Kirby P.A., 1999. Moment capacity and rotational stiffness of endplate connections to concrete-filled tubular columns with flowdrill connectors. *Journal of Constructional Steel Research*, 50, 35-48.

[5] Korol R.M., Ghobarah A., Mourad S., 1993. Blind bolting W-shape beams to HSS columns. *Journal of Structural Engineering*, 119, 3463-3481.

[6] Tabsh S.W., Mourad S., 1997. Resistance factors for blind bolts in direct tension. *Engineering Structures*, 19, 995-1000.

[7] Pitrakkos T., Tizani W., 2013. Experimental behaviour of a novel anchored blind-bolt in tension. *Engineering Structures*, 49, 905-919.

[8] Kurobane Y., Packer J.A, Wardenier J., Yeomans N., 2004. *Design guide for structural hollow section column connections.* Köln, Germany: CIDECT Verlag TÜV Rheinland.

[9] Park A.Y., Wang Y.C., 2010. Joint rotation behavior of bolted endplate connections to flowdrilled RHS columns. *13th International Symposium on Tubular Structures.* The University of Hong Kong, Hong Kong, China.

[10] Loh H.Y., Uy B., Bradford M.A., 2006. The effects of partial shear connection in composite flush end plate joints Part I-experimental study. *Journal of Constructional Steel Research*, 62, 378-390.

[11] Elghazouli A.Y., Malaga-Chuquitaype C, Castro J.M., Orton A.H., 2009. Experimental monotonic and cyclic behavior of blind-bolted angle connections. *Engineering Structures*, 31, 2540-2553.

[12] Wang J.F., Han L.H., Uy B., 2009. Hysteretic behavior of flush end plate joints to concrete-filled steel tubular columns. *Journal of Constructional Steel Research*, 65, 1644-1663.

[13] Wang J.F., Spencer Jr B.F., 2013. Experimental and analytical behavior of blind bolted moment connections. *Journal of Constructional Steel Research*, 82, 33-47.

[14] Wang Z.Y., Tizani W., Wang Q.Y., 2010. Strength and initial stiffness of a blind-bolt connection based on the T-stub model. *Engineering Structures*, 32, 2505-2517.

[15] Mesquita A.C.B., Simoes da Silva L.A.P., Jordao S., 2010. Behavior of I beam-SHS column steel joints with hollo-bolts: an experimental study. *13th International Symposium on Tubular Structures.* The University of Hong Kong, Hong Kong, China.

[16] Liu Y., Malaga-Chuquitaype C., Elghazouli A.Y., 2012. Response and component characterization of semi-rigid connections to tubular columns under axial loads. *Engineering Structures*, 41, 510-532.

[17] Liu Y., Malaga-Chuquitaype C., Elghazouli A.Y., 2012. Behavior of beam-to-tubular column angle connections under shear loads. *Engineering Structures*, 42, 434-456.

[18] Li D.X., Uy B., Aslani F., Patel V., 2017. Behaviour and design of demountable CFST column-column connections under tension. *Journal of Constructional Steel Research*, 138, 761-773.

[19] Li G.Q., Liu K., Wang Y.B., Dai Z.Q., 2019. Moment resistance of blind-bolted SHS column splice joint subjected to eccentric compression. *Thin-Walled Structures*, 141, 184-193.

[20] Wang W., Li M.X., Chen Y.Y., Jian X.G., 2017. Cyclic behavior of endplate connections to tubular columns with novel slip-critical blind bolts. *Engineering Structures*, 148, 949-962.

[21] Xu T., 2015. *Development of one-side bolt and experimental study on its connection behavior*. MASc. Tongji Universiy. (in Chinese)

[22] European Committee for Standardization, 2010. *EN 1993-1-1*: *Eurocode 3: Design of steel structures - Part 1-1: General rules and rules for buildings*, Brussels, Belgium.

[23] https://www.google.com/search?q=tor+shear+bolt&tbm=isch&source=univ&client=firefox-b-d&sa=X&ved=2ahUKEwjZppHqkqnnAhUv6XMBHZu_C3gQsAR6BAgIEAE&biw=1227&bih=564

[24] Chinese National Code, 2015. *GB 50010-2010*: *Code for design of concrete structures*, Beijing, China. (in Chinese)

[25] Chinese National Code, 2016. *GB 50011-2010*: *Code for seismic design of buildings*, Beijing, China. (in Chinese)

[26] American Institute of Steel Construction, 2016. *ANSI/AISC 341-16*: *Seismic provisions for structural steel buildings*, Chicago, USA.

[27] European Committee for Standardization, 2010. *EN 1993-1-8*: *Eurocode 3: Design of steel structures - Part 1-8: Design of joints*, Brussels, Belgium.

[28] Chinese Professional Code, 2015. *JGJ/T 101-2015*: *Specificating of testing methods for earthquake resistant building*, Beijing, China. (in Chinese)

[29] European Committee for Standardization, 2004. *EN 1994-1-1*: *Eurocode 4: Design of composite steel and concrete structures - Part 1-1: General rules and rules for buildings*, Brussels, Belgium.

[30] Timoshenko S., Woinowsky-Krieger S., 1959. *Theory of plates and shells*, McGraw-Hill Book Company, Singapore.

[31] Jiao W.F., 2019. *Research on behavior of square hollow-section steel tube to H-shaped beam with split-type spacer blind bolt in bolted end-plate connection*. PhD. Tongji Universiy. (in Chinese)

List of figure captions:

Fig.1. Components of a slip-critical blind bolt (SCBB)

Fig.2. Installation procedure of SCBB

Fig.3. Beam-to-column connection with 4 pairs of SCBBs

Fig.4. Specimen CB2, plan view

Fig.5.Details of RC slab

Fig.6. Schematic and actual test set-ups (a) Schematic test set-up for Specimens CB1 and CB2; (b) On-site test set-up of Specimen CB3

Fig.7. Loading protocol

Fig.8. Arrangements of LVDTs and strain gauges (a) For Specimens CB1 and CB2; (b) For Specimen CB3

Fig.9. Inter-storey drift θ for two extreme cases (a) No rigid body rotation of the column; (b) No rigid body rotation of the beam

Fig.10. Local buckling and fracture of Specimen CB1 (a) Beam local buckling at 0.05 rad; (b) Flange fracture at 0.06 rad

Fig.11. Torsional buckling and fracture of Specimen CB2 (a) Torsional buckling at 0.04 rad; (b) Flange fracture at 0.05 rad

Fig.12. Failures at the bottom flanges of Specimen CB3 (a) Significant local buckling deformations at 0.05 rad; (b) Bottom flange cracking and concrete crushing at 0.06 rad; (c) Complete fracture of bottom flange at 0.07 rad

Fig.13. No relaxation of SCBB connection

Fig.14. Hysteretic moment-rotation curves (a) CB1; (b) CB2; (c) CB3

Fig.15. Backbone curves

Fig.16. Stiffness degradation curves

Fig.17. Areas for calculating the equivalent viscous damping ratio

Fig.18. A simplified symmetric half of SHS column with two bolt loads

Fig.19. Mechanical model for $k_{fc,t,r}$ (a) Simplified diagram via centre line of cross-section; (b) Mechanical model for column flange; (c) Mechanical model for column web; (d) Three load cases for column flange

List of table captions:

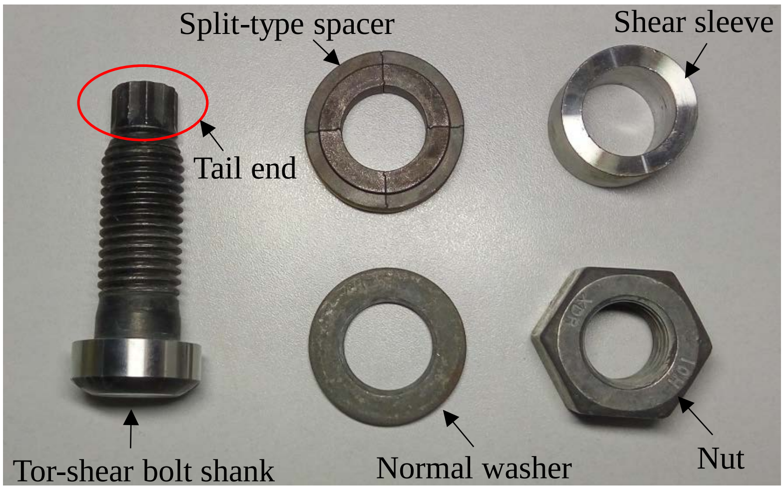

Fig. 1. Components of a slip-critical blind bolt (SCBB)

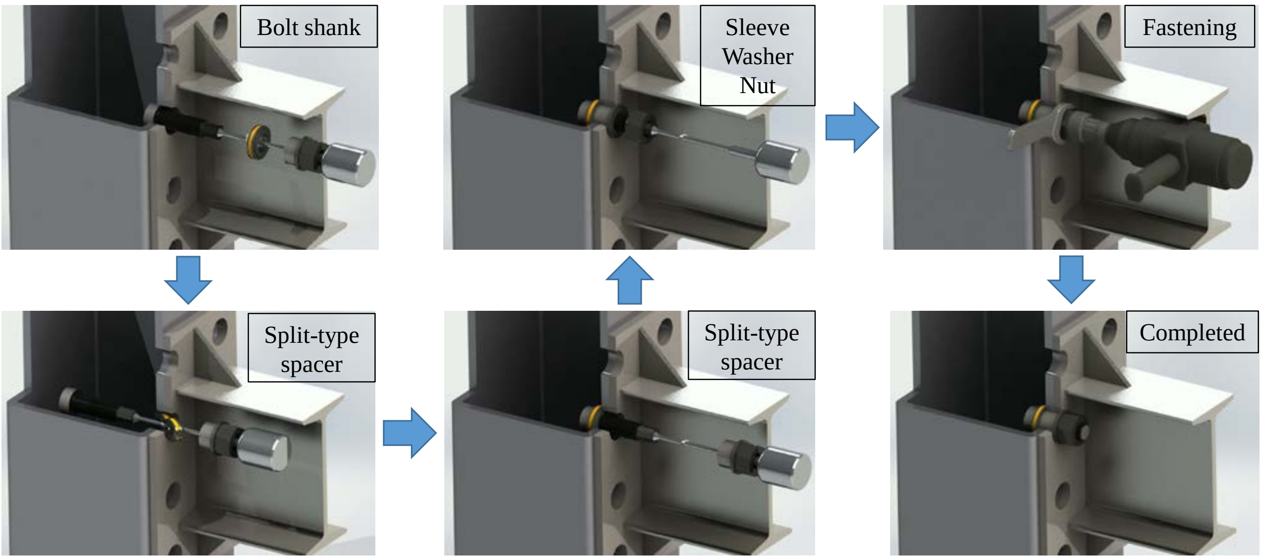

Fig. 2. Installation procedure of SCBB

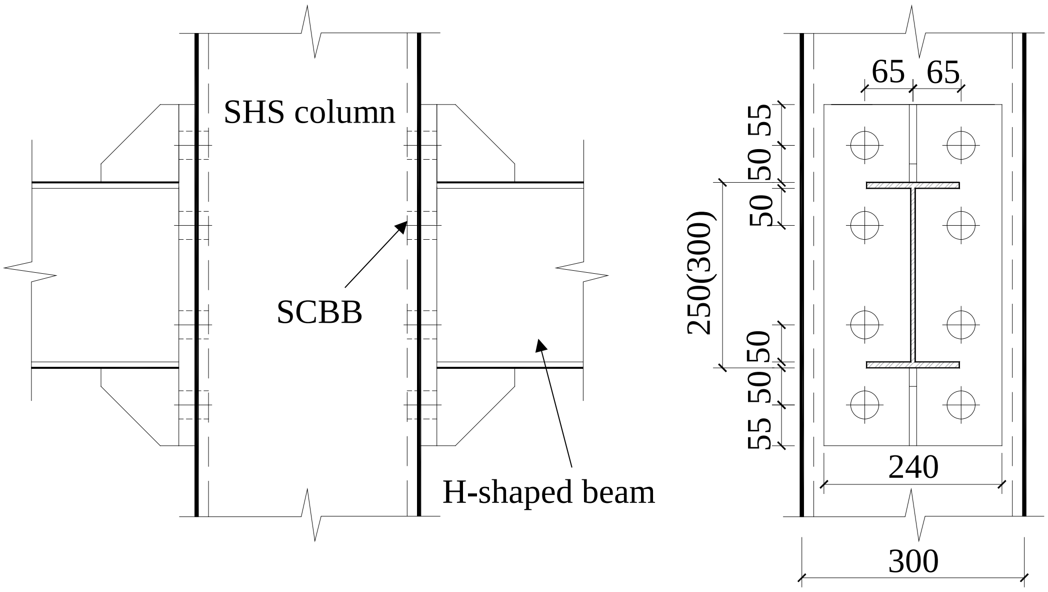

Fig. 3. Beam-to-column connection with 4 pairs of SCBBs

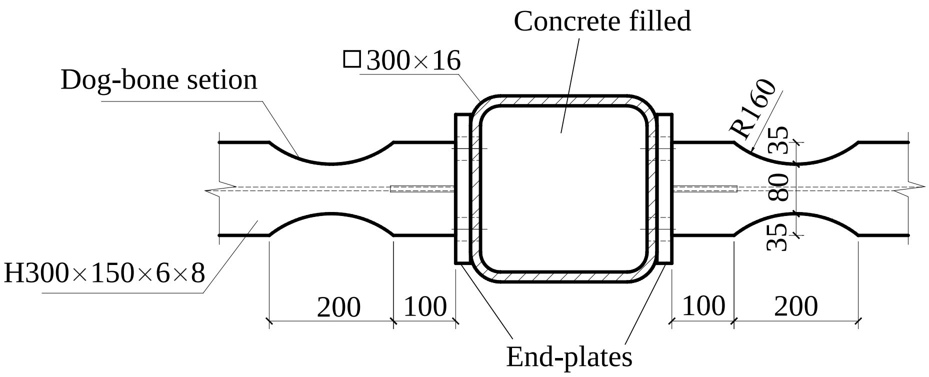

Fig. 4. Specimen CB2, plan view

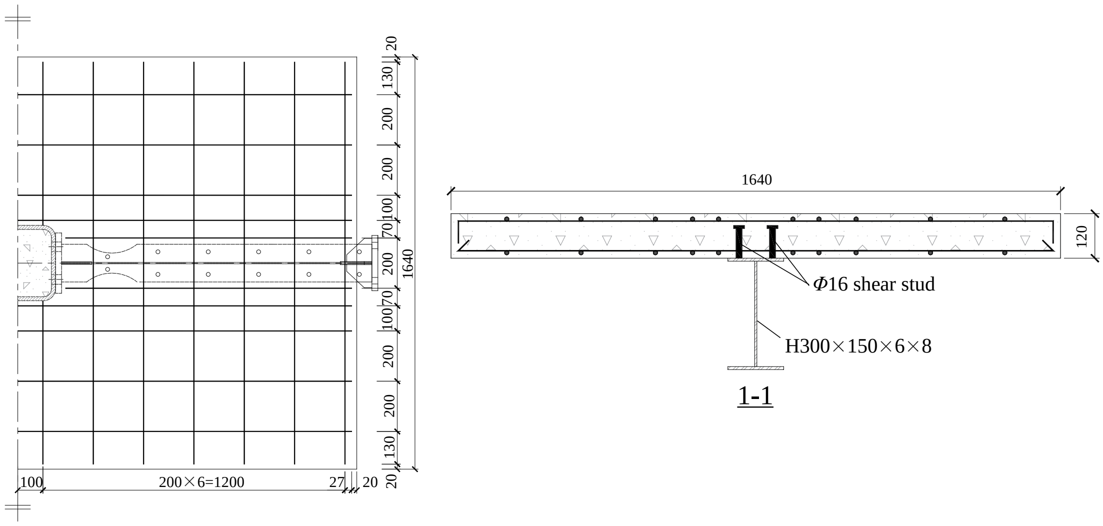

Fig. 5. Details of RC slab

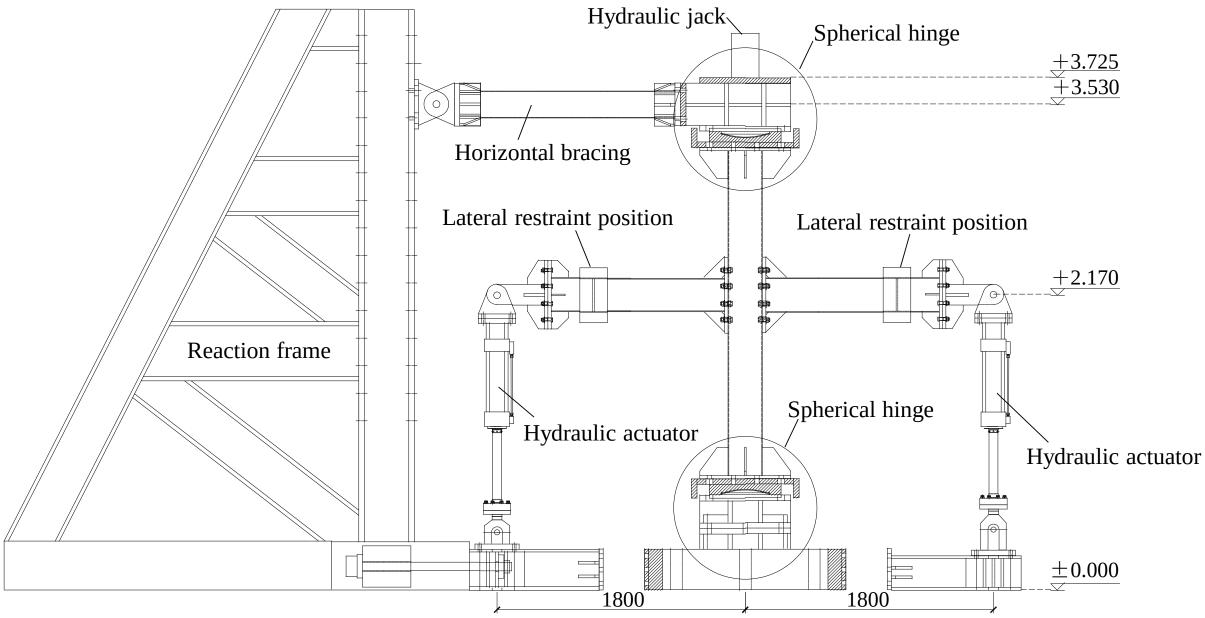

(a) Schematic test set-up for Specimens CB1 and CB2

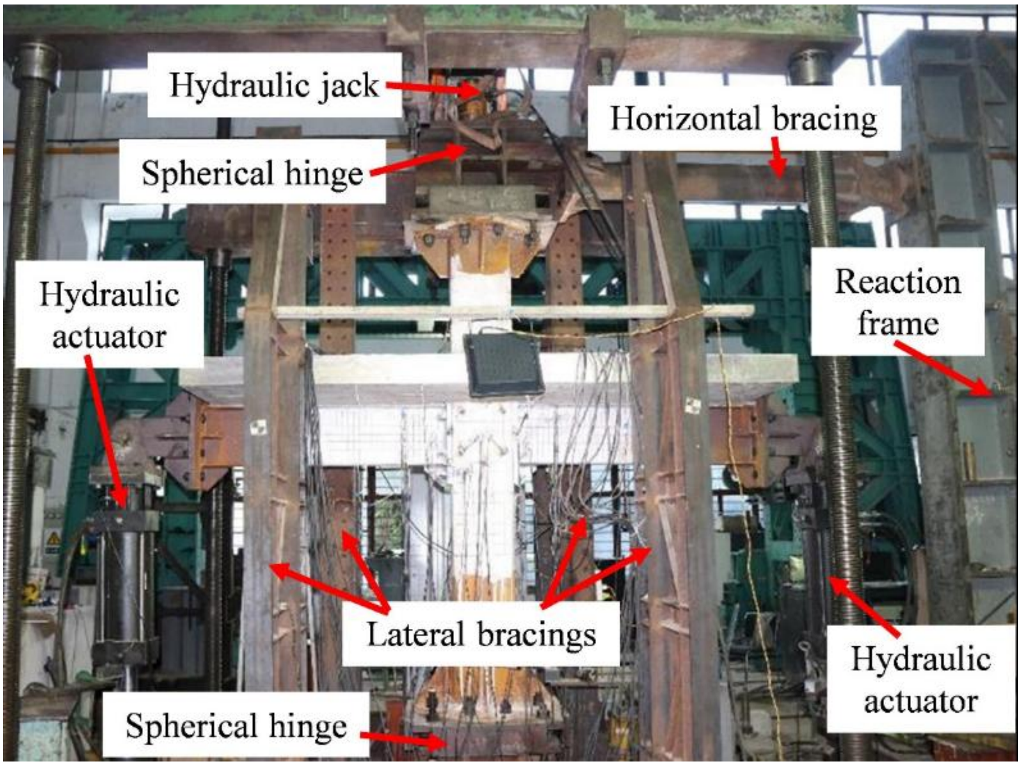

(b) On-site test set-up of Specimen CB3

Fig. 6. Schematic and actual test set-ups

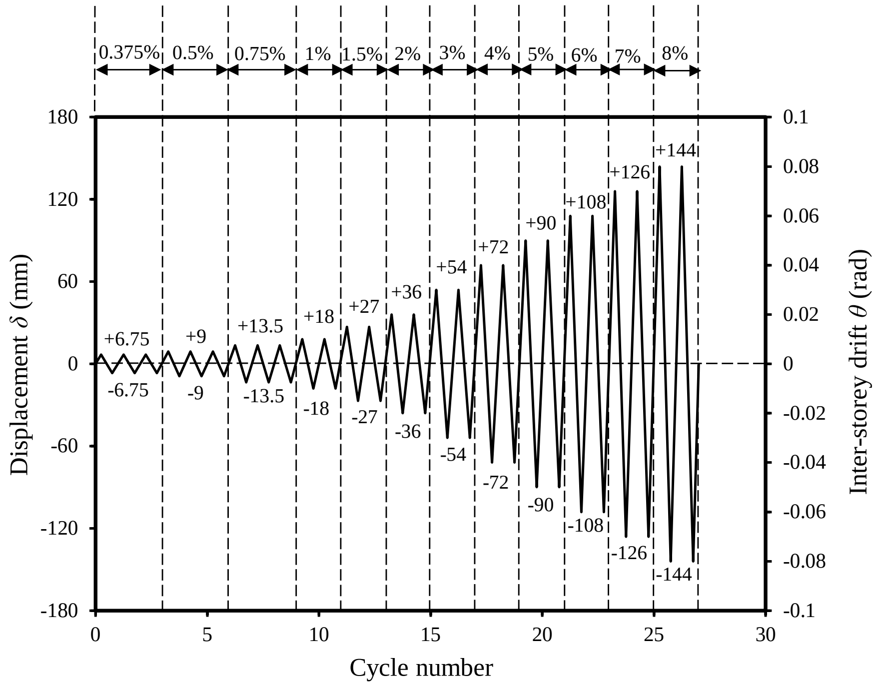

Fig. 7. Loading protocol

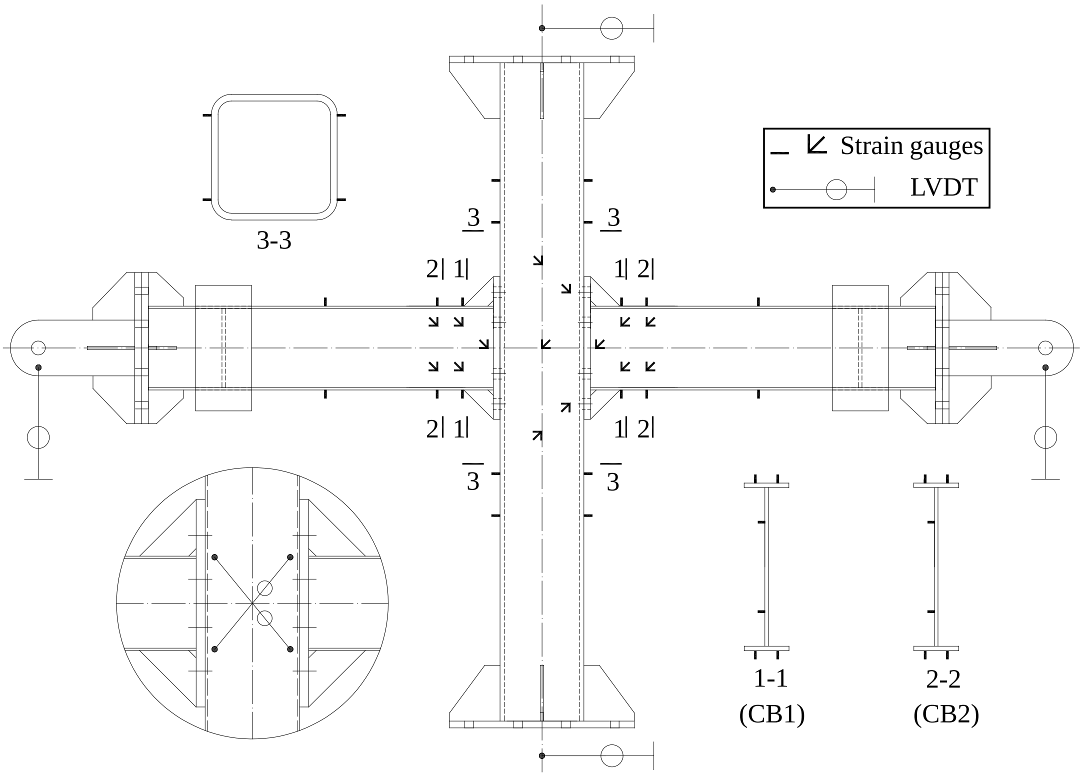

(a) For Specimens CB1 and CB2

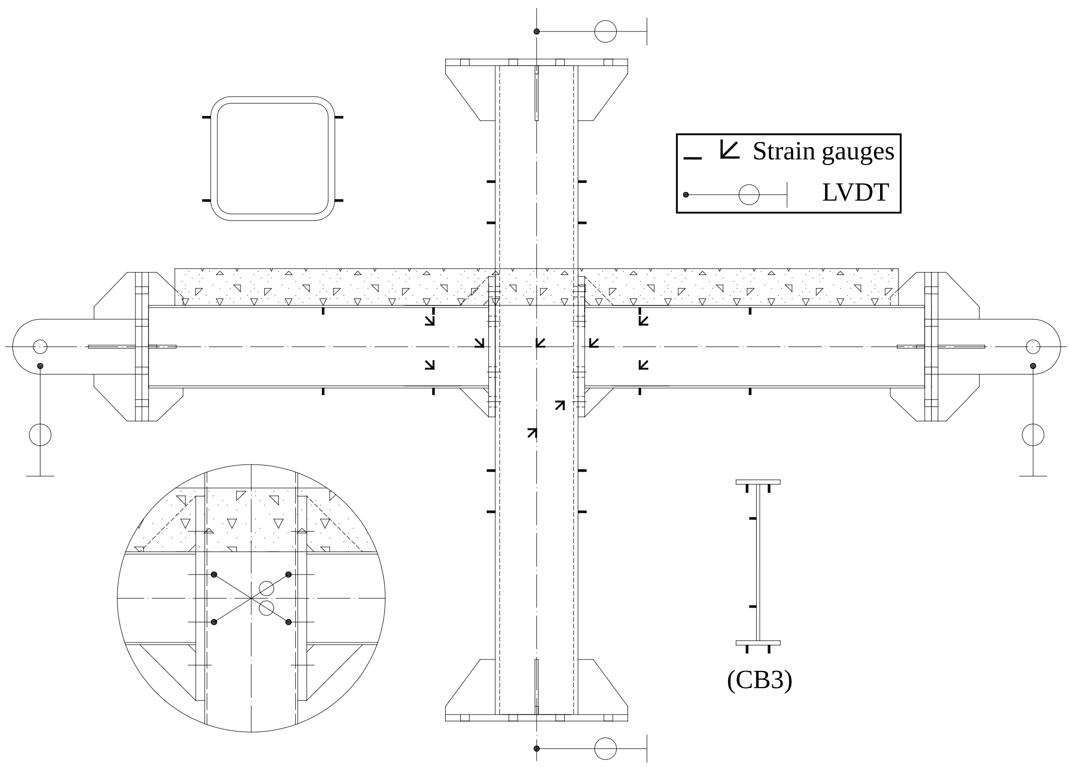

(b) For Specimen CB3

Fig. 8. Arrangements of LVDTs and strain gauges

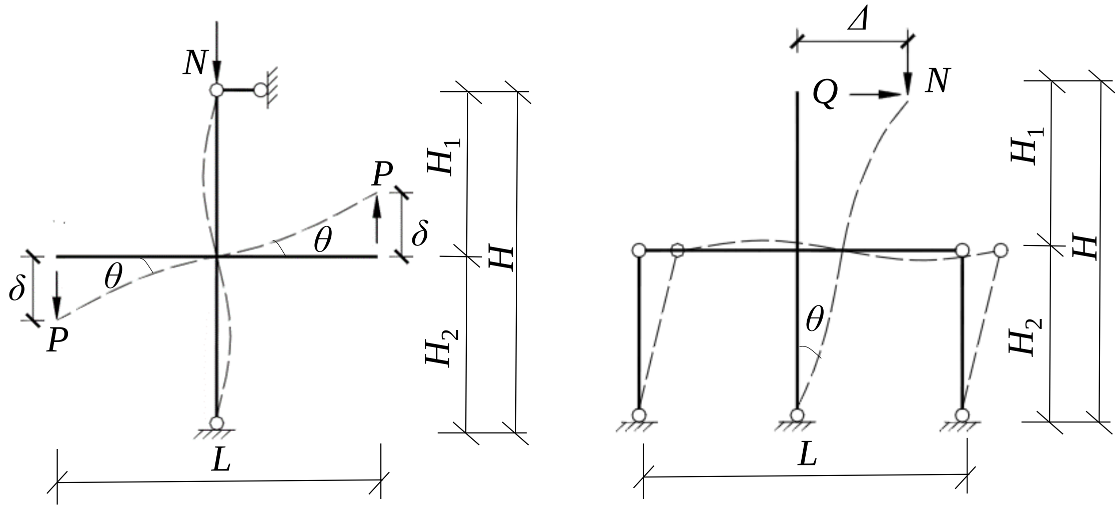

(a) No rigid body rotation of the column (b) No rigid body rotation of the beam

Fig. 9. Inter-storey drift θ for two extreme cases

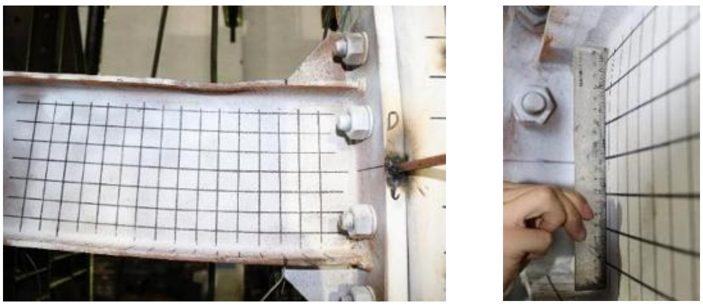

(a) Beam local buckling at 0.05 rad

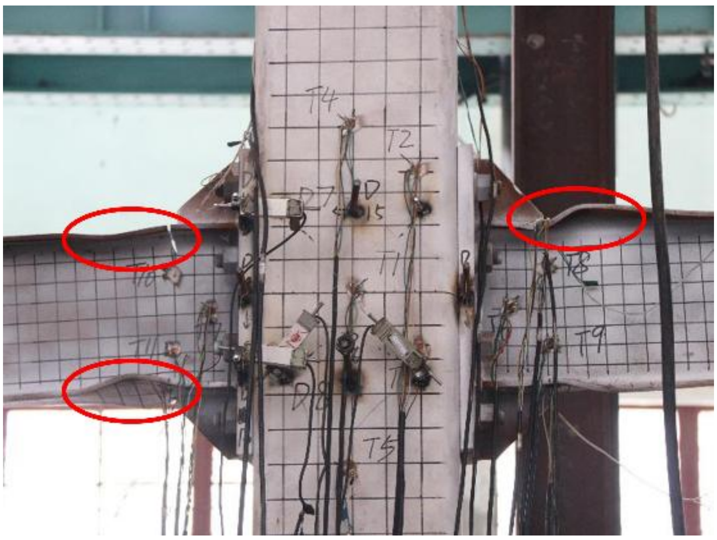

(b) Flange fracture at 0.06 rad

Fig. 10. Local buckling and fracture of Specimen CB1

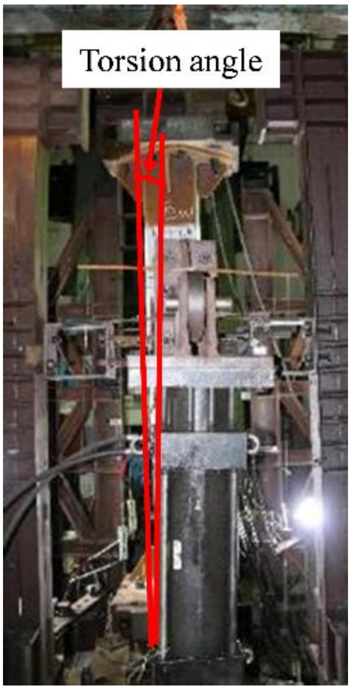

(a) Torsional buckling at 0.04 rad

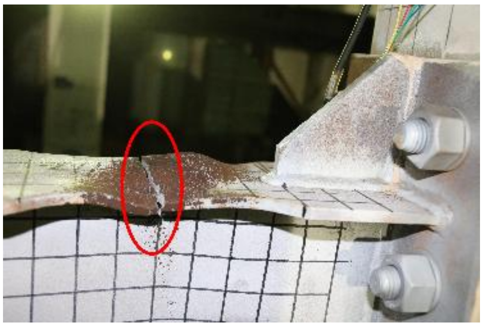

(b) Flange fracture at 0.05 rad

Fig. 11. Torsional buckling and fracture of Specimen CB2

(a) Significant local buckling deformations at 0.05 rad

(b) Bottom flange cracking and concrete crushing at 0.06 rad

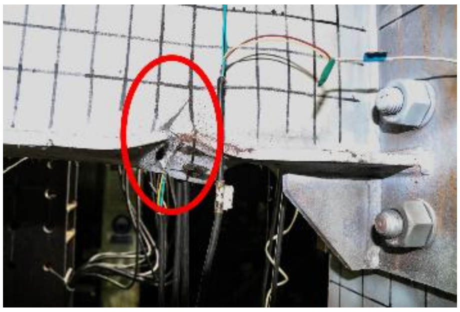

(c) Complete fracture of bottom flange at 0.07 rad

Fig. 12. Failures at the bottom flanges of Specimen CB3

Fig. 13. No relaxation of SCBB connection

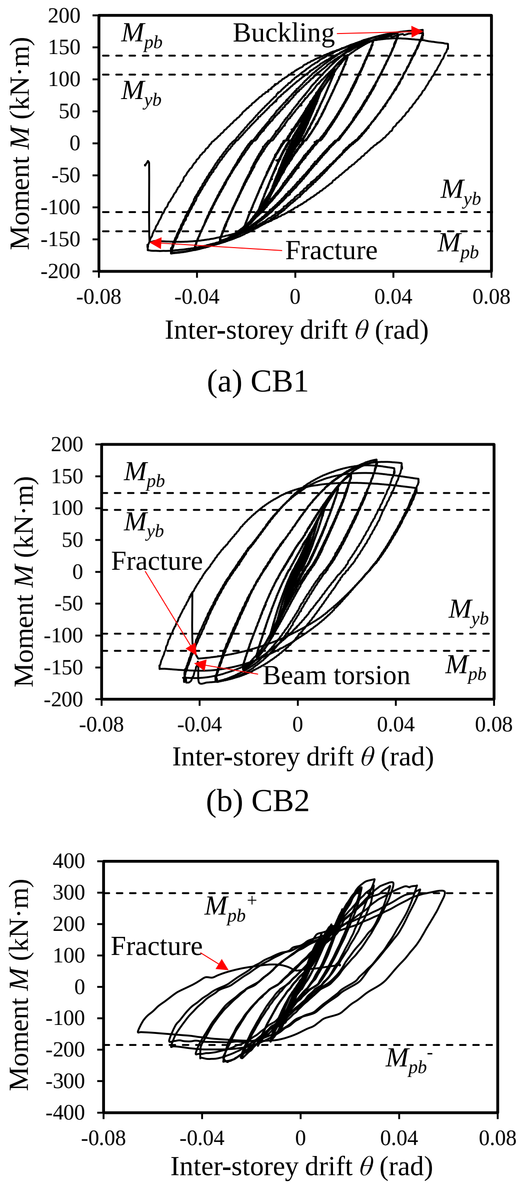

(a) CB1

(b) CB2

(c) CB3

Fig. 14. Hysteretic moment-rotation curves

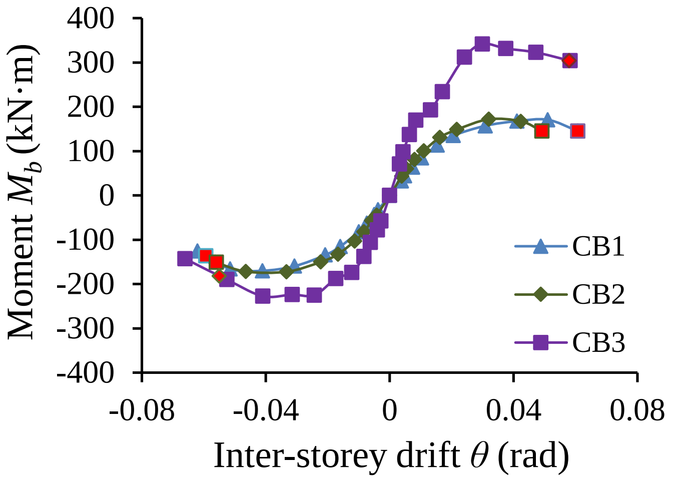

Fig. 15. Backbone curves

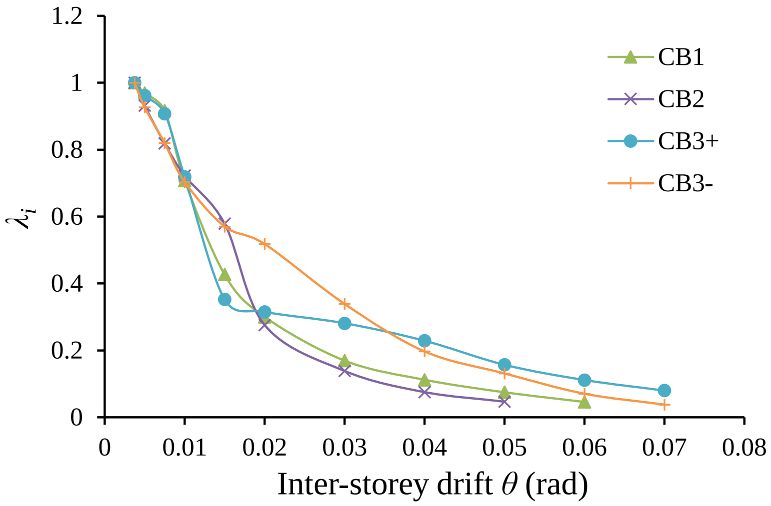

Fig. 16. Stiffness degradation curves

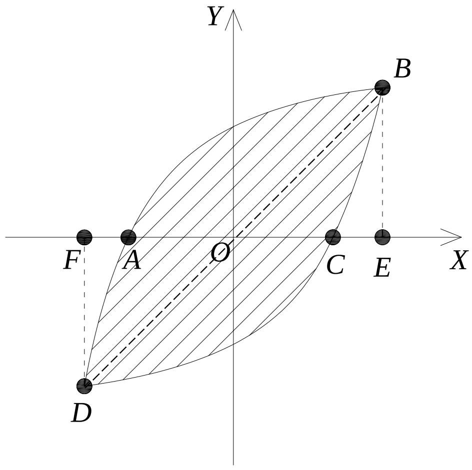

Fig. 17. Areas for calculating the equivalent viscous damping ratio

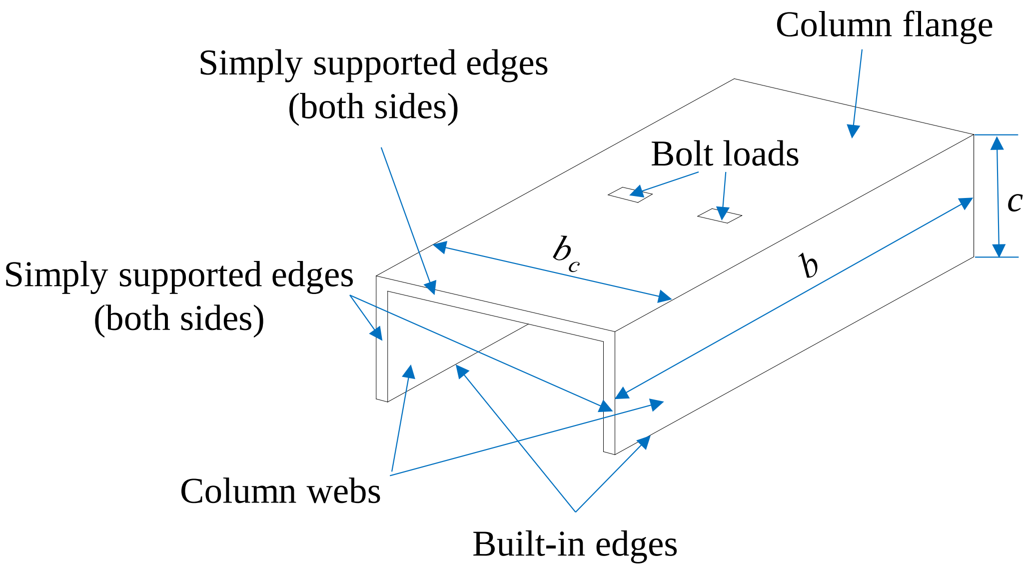

Fig. 18. A simplified symmetric half of SHS column with two bolt loads

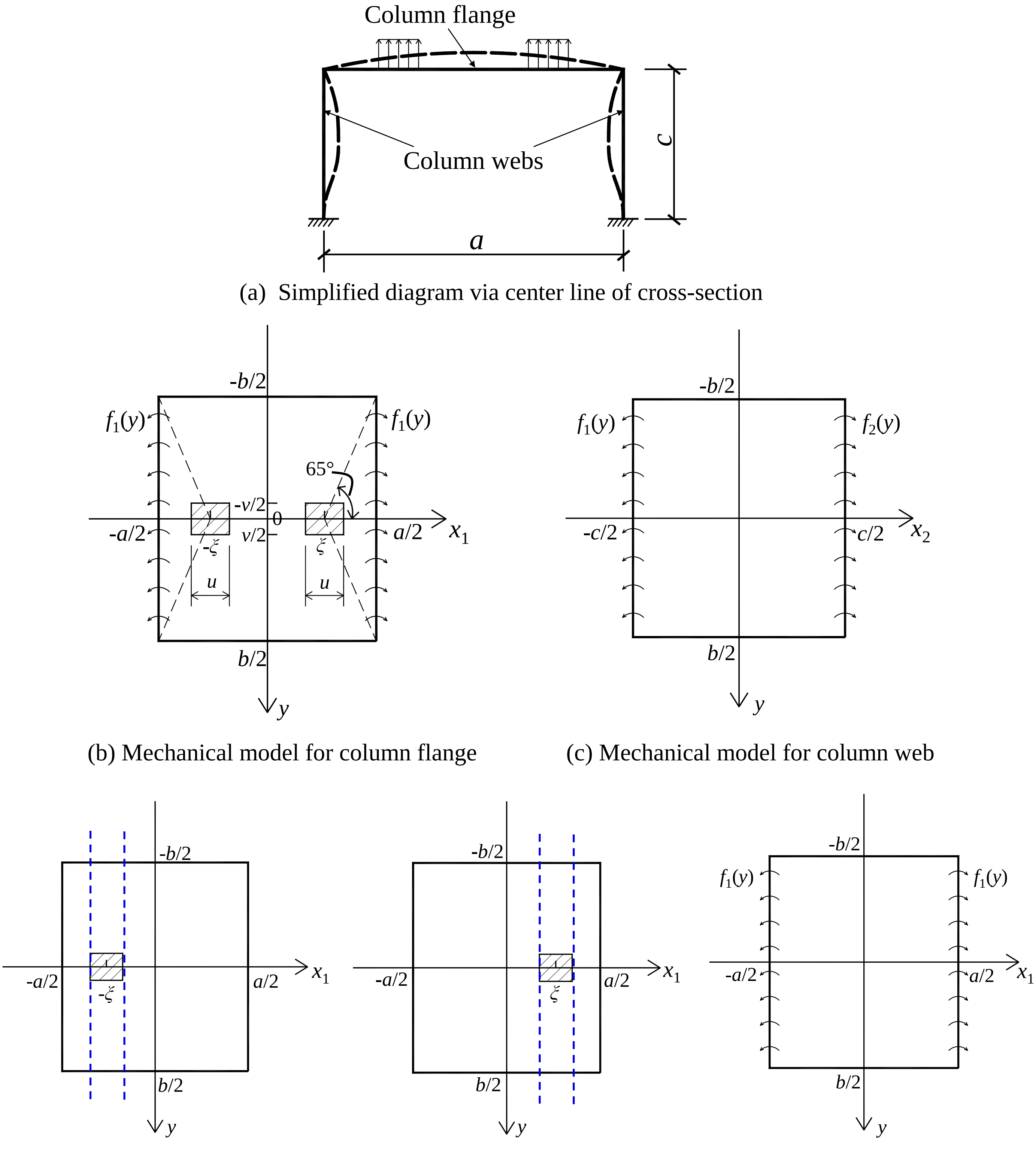

(a) Simplified diagram via center line of cross-section

(b) Mechanical model for column flange

(c) Mechanical model for column web

(d) Three load cases for column flange

Fig. 19. Mechanical model for $k_{fc,t,r}$

Table 1. Specimen configurations

Specimen	Column (mm) $b_c \times t_c \times L_c$	Beam (mm) $h_b \times b_b \times t_{wb} \times t_{fb}$	Axial load ratio n	Beam type
CB1	300×16×3035	250×125×6×8	0.1	Uniform welded section
CB2		300×150×6×8		Reduced section beam (RSB)
CB3				Concrete slab over RSB

Table 2. Material properties of steel sections and rebar

Steel type	F_y (MPa)	F_u (MPa)	Uniform elongation at fracture
Column	413	598	36%
Beam flange	380	519	34%
Beam web	414	570	32%
End-plate	417	601	39%
Reinforcing steel bar	504	703	39%

Table 3. Initial stiffness of test specimens and rigid joint thresholds

Specimen	S_{ini} (kN·m/rad)	$8EI_b/L_b$ (Braced)	$25EI_b/L_b$ (Unbraced)
CB1	54,838	11,766	36,771
CB2	46,027	17,201	53,753
CB3	78,188(+) 65,529(-)		

Table 4. Assessment of ductility

Specimen	$\theta_{0.8}$ (rad)	
	Positive direction	Negative direction
CB1	0.061	0.059
CB2	0.049	0.056
CB3	0.058	0.055

Table 5. Equivalent viscous damping ratio ζ_{eq}

Specimen	ζ_{eq}
CB1	0.469
CB2	0.476
CB3	0.389

Table 6. Stiffness coefficient of each component

$k_{i,r}$ (mm)		Specimen			
		CB1	CB2	CB3+	CB3-
$k_{1,r}$		26.9	26.6	27.1	27.1
$k_{2,r}$	$k_{2,1}$	29.0	28.8	28.7	28.7
	$k_{2,2}$	29.0	28.8	28.7	28.7
	$k_{2,3}$	27.1	27.0	26.8	26.8
$k_{3,r}$		9.83	9.83	9.83	9.83
$k_{4,r}$		None	None	None	2.39
$k_{5,r}$		0.804	0.774	0.836	0.836

Table 7. Comparison of initial rotational stiffness between analytical and experimental results

Specimen	$S_{j,ini,th}$ (kN·m/rad)	$S_{j,ini,test}$ (kN·m/rad)	Error
CB1	32,875	54,838	-40.1%
CB2	42,900	46,027	-7.3%
CB3	61,387+ 56,470-	78,188+ 65,529-	-21.4% -13.8%